

Relative contribution of submicron and supermicron particles to aerosol light scattering in the marine boundary layer

Christoph Kleefeld,¹ Colin D. O'Dowd,^{1,2,3} Sarah O'Reilly,¹ S. Gerard Jennings,¹ Pasi Aalto,² Edo Becker,³ Gerard Kunz,⁴ and Gerrit de Leeuw⁴

Received 15 December 2000; revised 12 August 2001; accepted 12 August 2001; published 4 September 2002.

[1] Measurements of the aerosol light scattering coefficient (σ_{sp}) at a wavelength of $\lambda = 550$ nm were conducted at a coastal atmospheric research station in the east Atlantic Ocean during June 1999. Size distribution measurements between diameters of 3 nm and 40 μm (at ambient humidity) were used to derive scattering coefficients from Mie theory. The calculated scattering coefficients were about a factor of 7.4 higher than the measured scattering coefficients. The discrepancy was explained by a reduced cutoff of the sampling system at particle diameters between 6 and 8 μm , dependent on wind speed. The calculated aerosol scattering was about 1 order of magnitude higher than previously reported measurements in the MBL and is attributed to supermicrometer particles at sizes $d > 10$ μm dominating aerosol scattering. *INDEX TERMS:* 0305

Atmospheric Composition and Structure: Aerosols and particles (0345, 4801); 0360 Atmospheric Composition and Structure: Transmission and scattering of radiation; 3359 Meteorology and Atmospheric Dynamics: Radiative processes; *KEYWORDS:* light scattering, sea-salt aerosol, marine boundary layer, particle size distribution, Mie theory

Citation: Kleefeld, C., C. D. O'Dowd, S. O'Reilly, S. G. Jennings, P. Aalto, E. Becker, G. Kunz, and G. de Leeuw, The relative contribution of submicron and supermicron particles to aerosol light scattering in the marine boundary layer (MBL), *J. Geophys. Res.*, 107(D19), 8103, doi:10.1029/2000JD000262, 2002.

1. Introduction

[2] Light scattering by atmospheric aerosol particles affects Earth's energy balance and contributes to the negative radiative forcing of climate. The overall impact of aerosols on the radiative balance comprises the absorption and scattering of radiation in the solar spectrum (direct effect) as well as the modification of the optical properties and lifetime of clouds (indirect effect). The quantification of these effects pose one of the largest uncertainties on the calculation of the global radiative forcing [*Intergovernmental Panel on Climate Change (IPCC)*, 1995]. The uncertainties are due to the complexity of the physical and chemical processes involving aerosol particles and due to the high temporal and spatial variability of their global and regional distribution. In this regard, measurements of aerosol optical properties are required on a regional scale, covering certain key areas.

[3] In the marine atmosphere, the typical background aerosol comprises primary produced sea salt particles and secondary produced particles consisting of non sea salt (nss) sulphate and organic compounds. The sea salt particles dominate the supermicrometer ($d > 1$ μm) part of the total aerosol size distribution spectrum whereas the nss sulphate particles fall within the submicrometer ($d < 1$ μm) range.

[4] Recent investigations however suggest that a fraction of the primary produced sea salt aerosol contributes significantly to the submicrometer portion of the particle size distribution [*O'Dowd and Smith*, 1993; *O'Dowd et al.*, 1997]. In terms of radiative forcing of climate, the submicrometer size range is most relevant for light scattering because it comprises particles with diameters comparable to the wavelength of the visible solar radiation. Measurements of the size segregated chemical composition of aerosols over the Southern Ocean and the application of Mie scattering theory to this data set confirmed the important role of submicrometer sea salt. Sea salt was found to dominate both the chemical composition and the aerosol light scattering of sub- μm particles [*Murphy et al.*, 1998].

[5] The relevance of sea salt aerosol for climatological processes stems from its radiative properties in conjunction with its production mechanism, which is highly wind speed-dependent. Climatic induced changes in wind speed pattern can affect the sea salt production and therefore alter the radiation balance over marine areas [*Latham and Smith*, 1990]. A competing process is the removal of sea

¹Department of Experimental Physics, National University of Ireland, Galway, Ireland.

²Department of Physics, University of Helsinki, Helsinki, Finland.

³Centre for Marine and Atmospheric Sciences, University of Sunderland, Sunderland, UK.

⁴Netherlands Organization for Applied Scientific Research, Physics and Electronics Laboratory, The Hague, Netherlands.

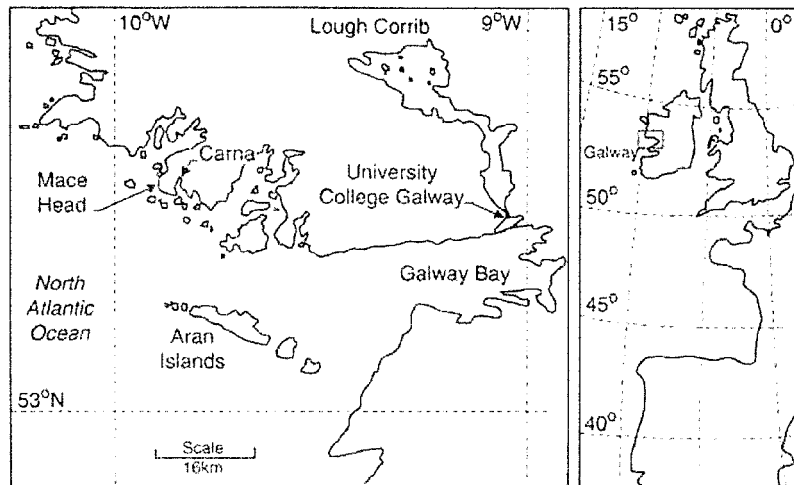


Figure 1. Map of the coastline features around the Mace Head measurement site.

salt aerosols by precipitation since precipitation patterns are also sensitive to climatic variations. In addition, sea salt contributes to the indirect radiation effect by serving as cloud condensation nuclei (CCN). A recent study by *O'Dowd et al.* [1999a] identifies sea salt aerosol as the primary source of CCN under high wind speed conditions in the marine boundary layer (MBL).

[6] Recently, the coastal zone was also identified as a strong source for secondary aerosol particles [*O'Dowd et al.*, 1999b, 1998]. The observed nucleation and growth processes are related to enhanced biological emissions of the intertidal zone during exposure to the atmosphere. The newly formed particles have the potential to grow into radiatively active sizes and thus could alter the radiation balance, which is most sensitive to perturbations over the low-albedo oceans [*O'Dowd*, 2002].

[7] A unique platform for studying marine aerosols is the Global Atmospheric Watch (GAW) atmospheric research station at Mace Head, located on the west coast of Ireland ($53^{\circ} 19' \text{ N}$, $9^{\circ} 54' \text{ W}$). The research station is situated at about sea level on a peninsula, which is surrounded by coastline and tidal areas except for a small sector ranging from 20° to 40° . The distance between the station and the shoreline is about 50 to 100 m in the westerly direction. A wind direction sector between 180° and 300° opens to the Atlantic Ocean and is associated with the advection of marine background air masses [*Jennings et al.*, 1997]. A map detailing the coastal features around Mace Head is shown in Figure 1.

[8] As part of the "New Particle Formation and Fate in the Coastal Environment" (PARFORCE) study, an intensive measurement campaign was conducted in Mace Head in June 1999. During this campaign a broad range of physical and chemical aerosol properties as well as meteorological parameters were simultaneously measured [*O'Dowd et al.*, 2002a]. Results are presented here from aerosol light scattering measurements in conjunction with Mie calculations of aerosol scattering coefficients. The contribution of background aerosols and local aerosol sources as well as the relative contribution of submicrom-

eter and supermicrometer particles to the light scattering coefficient will be examined.

2. Methods

2.1. Measurements

2.1.1. Aerosol Scattering Coefficient

[9] The aerosol scattering coefficient (σ_{sp}) was measured with a TSI Model 3551 single wavelength ($\lambda = 550 \text{ nm}$) integrating nephelometer. The instrument was connected via a 25 mm diameter duct to a community air-sampling system. The system was constructed from a 100 mm diameter stainless steel pipe and reached a height of 10 m above ground level. A flow rate of 250 l/min was maintained in the sampling pipe. A size fractionation of the aerosol at the sample inlet of the nephelometer was not conducted. Due to the internal heating of the nephelometer, aerosol was sampled at an average relative humidity (RH) of $41 \pm 7\%$.

[10] At the beginning and end of the campaign, the nephelometer was calibrated with particle-free air as the low span gas, and carbon dioxide as the high span gas. An automatic zero calibration with particle-free air was performed every 60 min for setting the instrument zero. The instrument noise is assessed as the standard deviation of the zero baseline measurements in order to determine the detection limit of the nephelometer. The mean detection limit of the nephelometer amounts to 0.3 Mm^{-1} as defined by a signal-to-noise ratio of 2. A detailed discussion of the performance characteristics of this commercial instrument is given by *Anderson et al.* [1996].

[11] The scattering coefficients were recorded with a temporal resolution of 5 min. These data were integrated to hourly arithmetic mean scattering coefficients.

2.1.2. Aerosol Number Size Distribution

[12] Information about the aerosol particle size distribution was obtained by means of electrical mobility analysis and optical particle counters, sampling the aerosol at a height of 10 m. Within the particle diameter range from 3 to 800 nm, the size distribution was measured by using two Differ-

ential Mobility Particle Sizer (DMPS) systems. The systems consisted of two Vienna type Differential Mobility Analyzers (DMA) and two condensation particle counters (TSI Models 3010 and 3025). Details of the instrument set up are presented by *O'Dowd et al.* [2002b]. The DMPS system was operated with a separate inlet system and not connected to the community air-sampling system. A Forward Scattering Spectrometer Probe (FSSP-100, PMS) provided in situ measurements of size distributions covering (wet) particle diameters from 0.5 to 47.0 μm [*Exton et al.*, 1985].

2.2. Calculation of Aerosol Scattering Coefficient

[13] In order to elucidate uncertainties associated with the measurement of aerosol light scattering coefficient the observed scattering coefficients are compared to calculated values derived from the Mie theory on the scattering of light from homogeneous spherical particles.

[14] The optical properties of atmospheric aerosols are dependent upon the particle size, the particle shape, the complex refractive index of the particle's chemical components, and upon the wavelength of the incident light. The scattering coefficient σ_{sp} can be mathematically expressed as an integral over all particle sizes in assuming spherical particles:

$$\sigma_{sp} = \int_{D=0}^{\infty} \frac{\pi D^2}{4} Q_{sca}(\lambda, m, D) \frac{dN}{d \log D} d \log D \quad (1)$$

where Q_{sca} is the dimensionless single particle efficiency factor for scattering, which depends on the wavelength λ of the light, the aerosol complex refractive index $m = n - ik$, where n is the real index of refraction and k is the imaginary index of refraction, and the particle diameter D . The particle number size distribution is denoted by $dN/d \log D$. The scattering efficiency is obtained from Mie theory and in order to facilitate the computation, Q_{sca} is expressed by the following algorithm [*Bohren and Huffman*, 1983]:

$$Q_{sca} \approx \frac{2}{x^2} \sum_{j=1}^N (2j+1) (|a_j|^2 + |b_j|^2) \quad (2)$$

[15] The dimensionless size parameter $x = \pi D/\lambda$ is calculated for the nephelometer wavelength of $\lambda = 0.55 \mu\text{m}$. The series a_j and b_j are defined by Ricatti-Bessel functions with the size parameter and the complex refractive index as variables. Equation (2) assumes an external mixture of the aerosol population.

[16] The aerosol number size distribution is obtained from DMPS and FSSP measurements. The Mie calculations based on the FSSP data have been restricted to particles with a (wet) diameter of less than 39.6 μm .

[17] Throughout the calculations, the aerosol volume is assumed to be dominated by sea salt particles (99%). In accordance with findings by *Jennings et al.* [1997] 1% of the total volume is attributed to black carbon (BC). The BC fraction is representative for clean marine air masses [*Van Dingenen et al.*, 1995; *O'Dowd et al.*, 1993] and originates from the long-range transport of combustion products. The associated refractive indices are taken from *Kent et al.* [1983]: $m = 1.5 - 10^{-8}i$ (sea salt) and $m = 1.75 - 0.44i$

(BC). The refractive index of water ($m = 1.333 - 10^{-9}i$) has to be considered in order to account for humidity effects, as detailed below.

[18] More recently, concentrations of organic carbon compounds have been reported for marine air masses at Mace Head, covering a summer period in 1998 [*Krivácsy et al.*, 2001]. On average, organic carbon compounds contribute about 9% to the total aerosol mass. Since the real part of the refractive index for organic material is given by 1.4 [*Horvath*, 1998] and therefore is comparable to the sea salt value of 1.5, the contribution of organic carbon compounds to the aerosol composition has not been considered within the Mie computation.

[19] A comparison between the measured and calculated aerosol scattering coefficients can be biased by not considering humidity effects. The total size distribution spectrum used for the scattering calculations is composed of measurements both at ambient relative humidity conditions (FSSP) and at dry conditions (DMPS). In order to adjust the size distribution data to the nephelometer humidity a parameterization by *Hänel* [1976] is introduced, relating the equilibrium radius of a particle and the relative humidity:

$$r_{\%RH} = r_0 \left(1 + \frac{\rho_0}{\rho_w} \frac{m_w}{m_0} \right)^{1/3} \quad (3)$$

where $r_{\%RH}$ and r_0 are the particle radius at a given relative humidity and the dry particle radius, respectively, ρ_0 denotes the mean density of the dry aerosol particle, ρ_w is the density of water and the ratio m_w/m_0 gives the mass of water condensed on the particle per unit mass of the dry substance. The parameters ρ_0 and m_w/m_0 were determined by *Hänel and Lehmann* [1981] for marine aerosols during a measurement campaign in Mace Head. The measured density ρ_0 amounts to $1.93 \pm 0.04 \text{ g/cm}^3$; the ratio m_w/m_0 varies between 0.0016 and 10.8 for a relative humidity range from approximately 22% to 96%. These values are based on the analyses of bulk aerosol samples that comprise particles with dry radii ranging from 0.15 to 5 μm .

[20] The dependence of the refractive index and hence the scattering coefficient on relative humidity can be expressed by an equation similar to equation (3), [*Hänel*, 1976]:

$$n_{\%RH} = n_w + (n_0 - n_w) \left(1 + \frac{\rho_0}{\rho_w} \frac{m_w}{m_0} \right)^{-1} \quad (4)$$

where $n_{\%RH}$ and n_0 denote the refractive index at a given relative humidity and at RH = 0%, respectively; n_w is the refractive index of water. In order to adjust the calculated scattering coefficients to the nephelometer humidity, the refractive index of the sea salt fraction is varied with relative humidity according to equation (4). The humidity correction is based on hourly averages of the measured ambient and nephelometer relative humidity. Throughout the campaign the ambient relative humidity varied between 54 and 95%, with a mean value and standard deviation of $79\% \pm 9\%$.

[21] A potential uncertainty inherent in the calculated scattering coefficients derives from the assumption of spherical particles that is required by Mie theory. At the nephelometer relative humidity particles may not be per-

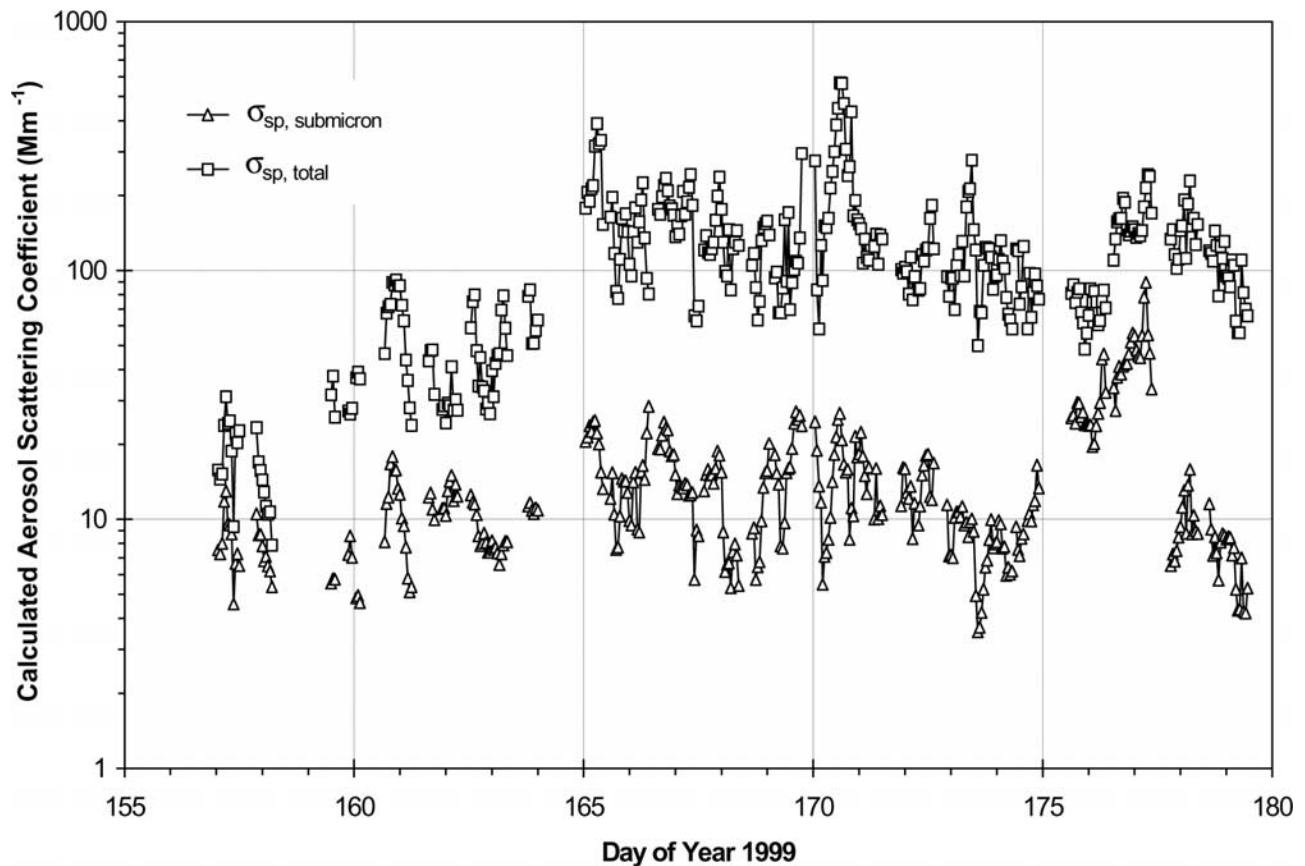


Figure 2. Time series of the calculated total ($\sigma_{sp, total}$) and the calculated submicrometer ($\sigma_{sp, sub}$) aerosol scattering coefficient.

fectly spherical. NaCl has a crystallization relative humidity of 48 – 46% [Tang, 1996] and may contribute to a solid phase within the particle. The effect of such irregular shaped particles on light scattering is difficult to quantify. *Pilinis and Li* [1998] used the T-matrix method to estimate the scattering coefficients of randomly oriented oblate and prolate spheroids and compared the results with Mie calculated scattering coefficients. For submicrometer particles the assumption of spherical particles introduces errors less than 10% in the scattering coefficient. However, the error will increase with increasing particle diameter, resulting in an underestimation of the real scattering by the assumption of sphericity.

[22] In the following, the calculated total scattering coefficient ($\sigma_{sp, total}$) refers to Mie calculations based on the DMPS and the FSSP data whereas the calculated submicrometer scattering coefficient ($\sigma_{sp, sub}$) refers to Mie computations based on the DMSP data solely. The Mie calculations are performed with hourly averages of the DMSP and FSSP data to facilitate a comparison with the measured scattering coefficients.

3. Results and Discussion

3.1. Calculated Aerosol Scattering Coefficients

[23] The time series of the calculated total and submicrometer scattering coefficients are presented in Figure 2. The data cover the period from 6 June to 28 June, from day

of the year (DOY) 157 to 179 for the year 1999. The gaps in the time series are caused by missing size distribution data.

[24] The calculated total scattering coefficients vary between 7.8 and 567 Mm^{-1} with an arithmetic mean and standard deviation of $116.8 \pm 80.2 Mm^{-1}$. In marine air masses only, as defined by a local wind direction sector ranging from 180° to 300° [Jennings *et al.*, 1997], the mean aerosol scattering level is shifted to a higher value of $144.0 \pm 86.1 Mm^{-1}$. Representative total scattering coefficients of the unperturbed MBL as given by the IPCC [1995], cover a range from 5 to 20 Mm^{-1} . These values are about one order of magnitude lower than the total scattering coefficients calculated for Mace Head.

[25] However, the comparison has to be limited. Aerosol scattering measurements are typically performed with a particle diameter cutoff at $d = 10 \mu m$ under ambient relative humidity conditions. The Mie computation, however, used a maximum particle size of a (wet) diameter of 39.6 μm , as measured by the FSSP. The additional particle mass contributes to the observed discrepancy between MBL scattering coefficients and the calculated values. Although these coarse particles lie outside of the optically efficient size range their mass concentration compensates for the low scattering efficiency.

[26] The contribution of coarse particles to the total aerosol scattering is illustrated in Figures 3 and 4. A typical number size distribution under high and low wind speed conditions is presented in Figures 3a and b for the DOY 170

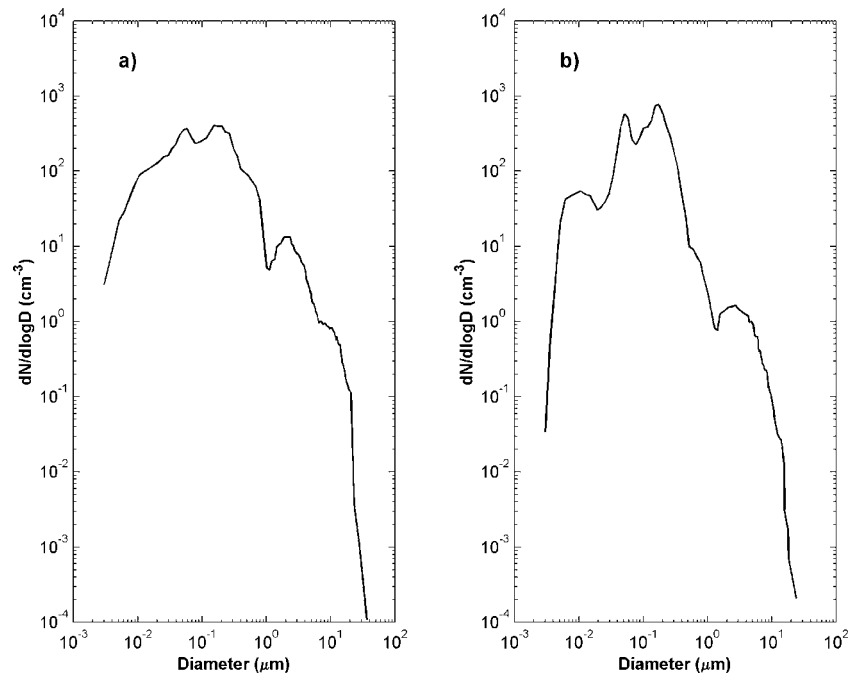


Figure 3. Hourly average of a number size distribution under (a) high wind speed (15 ms^{-1}) and (b) low wind speed (5 ms^{-1}) conditions for DOY 170 and 163, respectively.

and 163, respectively. The size distributions are based on hourly averages of the DMPS and FSSP measurements and cover particle diameters from 3 nm to about 25 μm . The particle diameters of the FSSP data have been humidity corrected and thus represent particle sizes at the nephelometer relative humidity. Assuming an ambient RH of 78%

and a nephelometer RH of 41%, the maximum (wet) particle diameter of 39.6 μm , used in the Mie calculation, will transform into a dry particle diameter of 22.9 μm . The number size distributions show a trimodal shape with maximum $dN/d\log D$ values in good agreement with previous measurements in the MBL over the open ocean

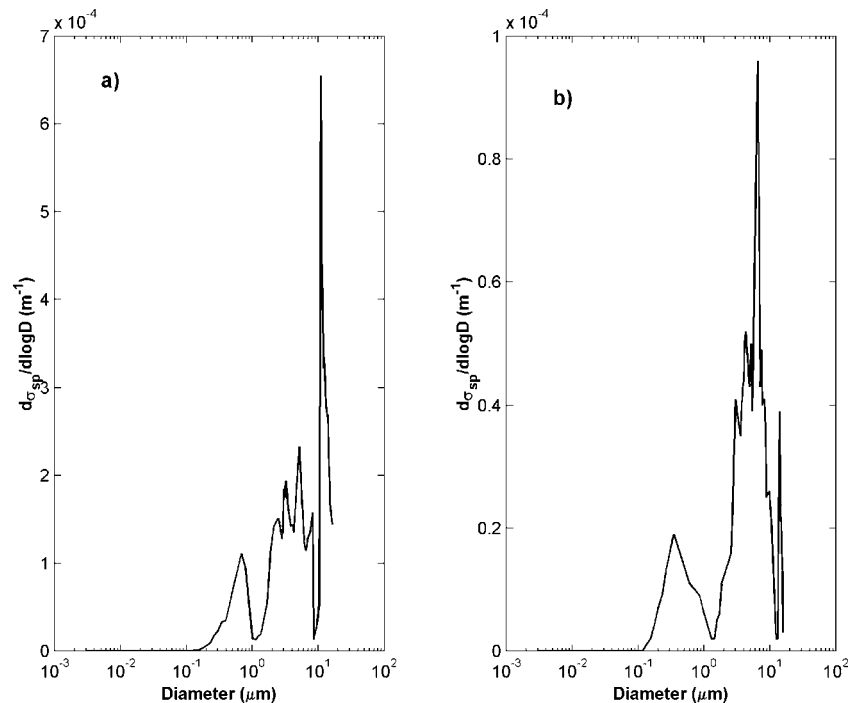


Figure 4. Hourly average of a calculated scattering coefficient size distribution ($d\sigma_{sp}/d\log D$) under (a) high wind speed (15 ms^{-1}) and (b) low wind speed (5 ms^{-1}) conditions for DOY 170 and 163, respectively. Note the different scales of the ordinates.

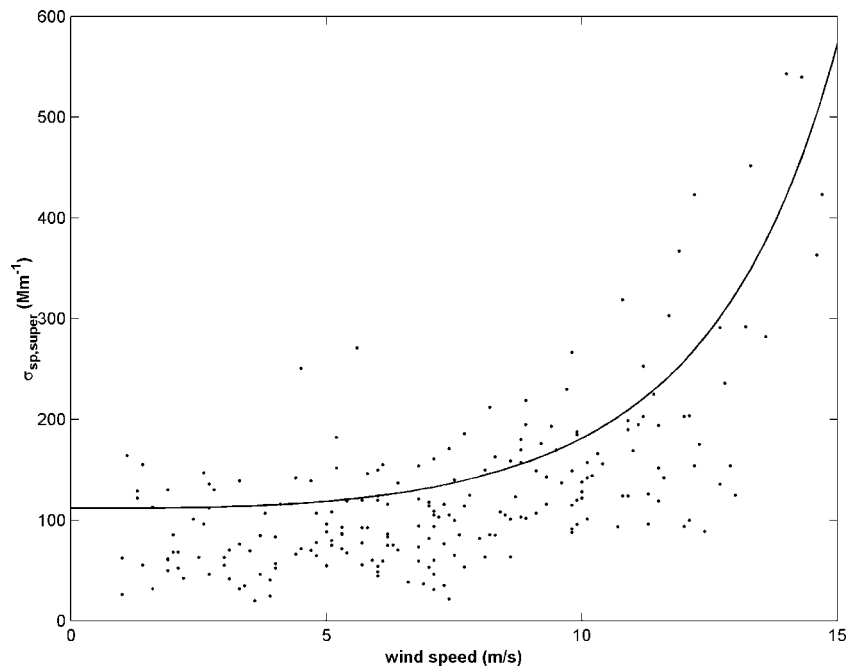


Figure 5. Calculated supermicrometer ($\sigma_{\text{sp, super}}$) scattering coefficient versus local wind speed for marine air masses. Inserted is an exponential regression line ($r^2 = 0.38$).

[O'Dowd *et al.*, 1997; Fitzgerald, 1991]. Therefore the observed size distributions can be regarded as representative for marine aerosols. The corresponding aerosol scattering coefficient size distribution ($d\sigma_{\text{sp}}/d\log D$) for DOY 170 and 163 is given in Figures 4a and b, respectively. Figure 4 corroborates that the aerosol scattering is dominated by supermicrometer particles under high wind as well as under low wind conditions. The maximum scattering occurs at dry particle diameters between 3 and 10 μm .

[27] The calculated submicrometer scattering coefficients, $\sigma_{\text{sp, sub}}$, as shown in Figure 2, vary between 3.5 and 89.5 Mm^{-1} with an average value and standard deviation of $14.6 \pm 11.0 \text{ Mm}^{-1}$. In marine air masses the average is slightly higher and amounts to $16.9 \pm 11.4 \text{ Mm}^{-1}$. These values are about a factor of 4 – 5 higher than results of comparable measurements of submicrometer scattering coefficients in the MBL [Quinn *et al.*, 1998; Anderson *et al.*, 1999].

[28] The discrepancy reflects the different cutoff diameters used in the MBL measurements and in the Mie calculations. The MBL measurements have been reported for a cutoff diameter of 1 μm under ambient relative humidity conditions while the Mie calculations have been performed for dried particles with $d < 0.8 \mu\text{m}$.

[29] In order to determine the relative contributions of submicrometer and supermicrometer particles to total scattering the submicrometer scattering fraction $F = \sigma_{\text{sp, sub}}/\sigma_{\text{sp, total}}$ has been calculated. The ratio F ranges from 0.03 to 0.68 with a mean value of 0.17 ± 0.13 . For marine background air masses arriving at Mace Head the average of F is slightly smaller and amounts to 0.14 ± 0.09 . The scattering fraction clearly indicates that the light scattering is dominated by supermicrometer particles.

[30] Since sea salt dominates the mass concentration of marine aerosols a correlation between wind speed and scattering would be expected. For marine air masses, the

calculated super- μm scattering fraction $\sigma_{\text{sp, super}} = \sigma_{\text{sp, total}} - \sigma_{\text{sp, sub}}$ is plotted versus the local wind speed in Figure 5. An exponential regression line is added to the figure. In general, the supermicrometer scattering increases with increasing wind speed, but the increase is more pronounced for wind speeds in excess of about 7 m/s. At about this wind speed the sea salt aerosol production due to the bursting of bubbles formed in whitecaps becomes significant [O'Dowd *et al.*, 1997] and hence contributes significantly to the sea salt mass concentration and to the light scattering. At wind speeds $< 7 \text{ m/s}$ the regression line indicates a fairly constant scattering level of about 110 Mm^{-1} , which is regarded as the background scattering signal. The overall coefficient of determination, r^2 , between local wind speed and $\sigma_{\text{sp, super}}$ is 0.38. The calculated submicrometer scattering, $\sigma_{\text{sp, sub}}$, and the local wind speed shows no correlation ($r^2 = 0.02$). However, a correlation between wind speed and scattering has to be limited. Apart from the local wind speed-dependent production mechanism, the local sea salt concentration will be influenced by a sea salt background. The poor correlation between local wind speed and $\sigma_{\text{sp, sub}}$ indicates either a significant contribution of nss sulphate to the sub- μm particle concentration or the dominance of advection processes. In particular, sub- μm particles can be transported over long distances due to their atmospheric residence time of several days.

3.2. Comparison of Calculated and Measured Scattering Coefficients

[31] A comparison between the measured and the calculated total light scattering coefficients is presented in Figure 6. The figure reveals a clear discrepancy between the measured σ_{sp} and the calculated $\sigma_{\text{sp, total}}$ values. The calculated total light scattering coefficients are an average factor of 7.4 ± 3.4 higher than the measured σ_{sp} values. However, both time series show similar trends, which is

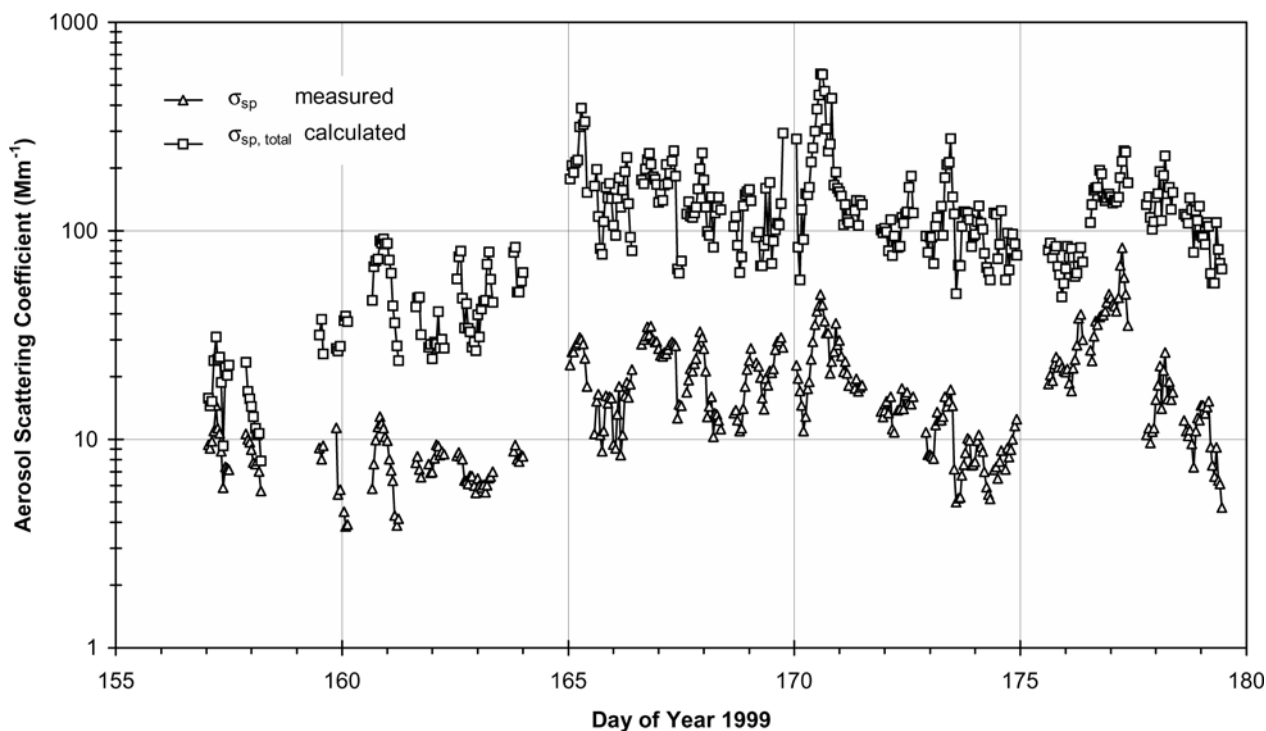


Figure 6. Comparison between the time series of the calculated total aerosol scattering coefficient ($\sigma_{sp, total}$) and the measured aerosol scattering coefficient (σ_{sp}).

expressed by a coefficient of determination, r^2 , of 0.41, resulting from a linear regression. The observed discrepancy indicates that the nephelometer significantly underestimates the light scattering if the whole particle size range covered by the DMPS and FSSP measurements is taken into account.

[32] With increasing particle diameter scattering becomes more pronounced in the near-forward direction, which cannot be efficiently sensed by the nephelometer due to its geometry. In a study by *Anderson and Ogren* [1998] the underestimation of light scattering by coarse particles of diameter 1.0 to 10 μm amounts to a mean factor of about 1.5. *White et al.* [1994] found a mean correction factor of about 2 for particles between 2.5 and 15 μm of diameter. Since the magnitude of these factors are smaller than the mean $\sigma_{sp, total}/\sigma_{sp}$ ratio of 7.4 the observed discrepancies cannot be explained by the angular truncation error of the nephelometer alone.

[33] The differences between the calculated submicrometer scattering $\sigma_{sp, sub}$ and the measured scattering σ_{sp} are much smaller and the mean ratio $\sigma_{sp, sub}/\sigma_{sp}$ amounts to 0.9 ± 0.3 , indicating on average of 10% higher measured scattering coefficients. A linear regression between both data sets results in a coefficient of determination of $r^2 = 0.76$. This reasonable agreement between calculated and measured scattering values is found if larger particles ($d > 0.8 \mu\text{m}$) are omitted from the Mie calculation, that is, to use solely the DMPS data for the computation. Therefore the nephelometer measurements reflect the light scattering of the dry submicrometer particle spectrum rather than the light scattering of the total dry particle size spectrum. However, a ratio of $\sigma_{sp, sub}/\sigma_{sp} < 1$ in conjunction with similar trends in the $\sigma_{sp, total}$ and σ_{sp} time series imply that a

fraction of supermicrometer particles with diameters $> 0.8 \mu\text{m}$ are detected by the instrument.

[34] In order to determine the aerosol losses of the sampling system and to estimate the nephelometer cutoff diameter, the efficiency η :

$$\eta = \frac{C}{C_0} \quad (5)$$

where C_0 denotes the ambient concentration and C is the sampled concentration of a certain particle size, is calculated from empirical relationships given by *Willeke and Baron* [1993]. The total efficiency of the sampling system is the product of the inlet efficiency and the transport efficiency of the sampling line. The inlet efficiency consists of the aspiration efficiency, that is the amount of particles entering the inlet, and the transmission efficiency, that is the fraction of aspirated particles reaching the sampling line. The calculation of the transport efficiency takes into account the loss of particles due to inertial depositions in the 90° bend of the sampling line as well as in the flow constriction at the nephelometer duct. In addition, the particle loss due to gravitational settling within the 5-m horizontal part of the sampling line is calculated.

[35] The resulting total efficiency of the sampling system as a function of particle diameter is presented in Figure 7 for three different wind speeds of 5, 10, and 15 m/s. About 90% of all hourly wind speed means of the measurement period are ≤ 10 m/s and about 52% of all mean values range between wind speeds of 5 and 10 m/s. Figure 5 reveals that particle losses occur both in the submicrometer fraction and in the supermicrometer fraction of the size spectrum. For wind speeds ≤ 10 m/s, up to 20% of the submicrometer

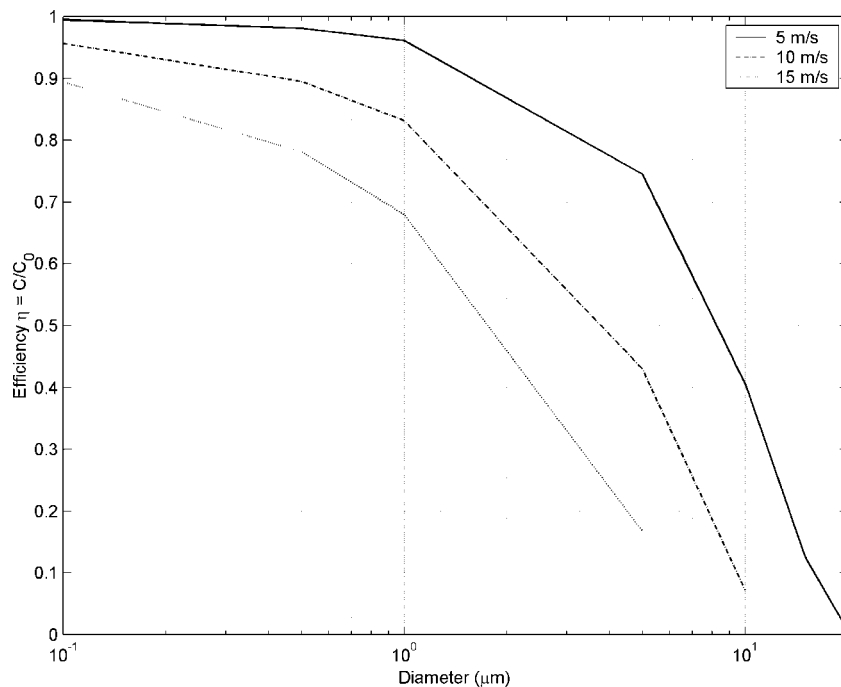


Figure 7. Total efficiency of the sampling system as a function of particle diameter for three different wind speeds of 5, 10, and 15 m/s.

particles will be removed from the sampling volume. The 50% cutoff diameter of the sampling system is about 8 μm at low wind speed conditions and decreases to about 4 μm at wind speeds of 10 m/s.

[36] The estimated particle losses at the sampling inlet and in the sampling line will contribute to the observed

discrepancies between measured and calculated scattering coefficients.

3.3. Measured Scattering Coefficients

[37] The measured aerosol scattering data are shown in Figure 8. The time series of σ_{sp} covers the period from 5

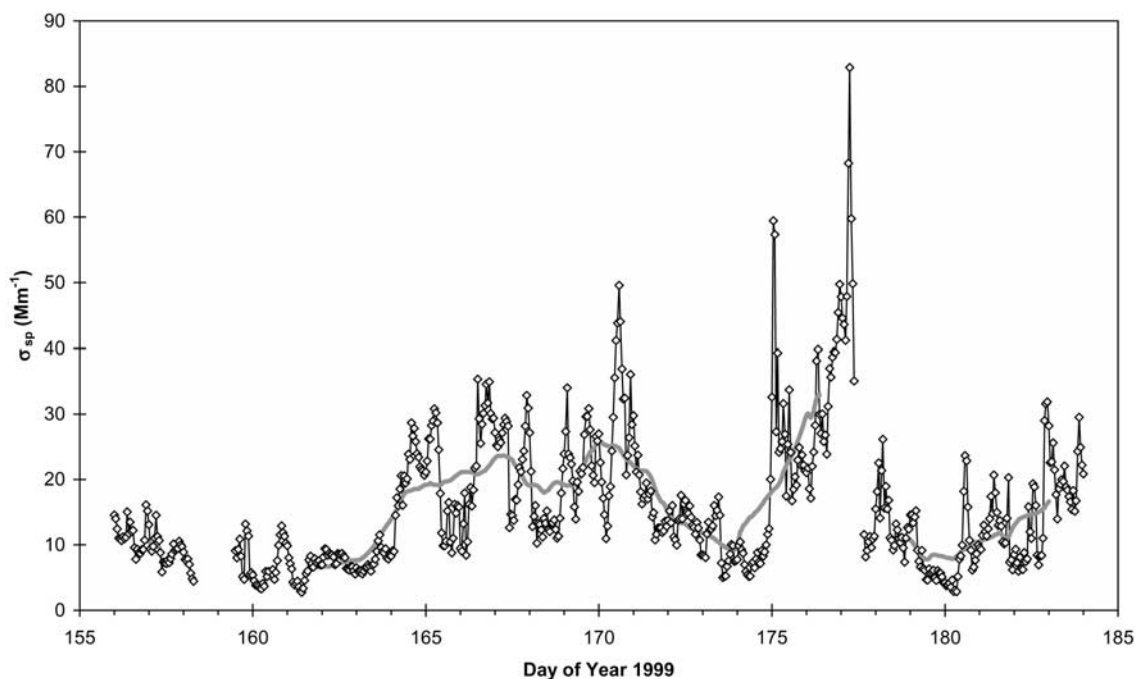


Figure 8. Time series of measured aerosol scattering coefficient (σ_{sp}). The shaded line indicates a 2-day moving average.

June to 2 July 1999 (DOY 156 – 183). Each data point represents an arithmetic hourly average. An interpretation of this data set has to consider that the true light scattering is underestimated by the measured σ_{sp} values due to submicrometer and supermicrometer particle losses in the sampling system, as mentioned above.

[38] The measured scattering coefficients range from 2.8 to 82.9 Mm^{-1} , resulting in a mean value and standard deviation of $15.7 \pm 10.3 Mm^{-1}$. The mean scattering level is higher, only if marine air masses arriving at Mace Head are taken into account. In these air masses, mean σ_{sp} amounts to $20.8 \pm 11.5 Mm^{-1}$. During the measurement period, marine air masses are associated with a moderate mean wind speed of 6.8 ± 3.0 m/s. The sampling efficiency at this wind speed is calculated to $> 90\%$ for submicrometer particles and the 50% cutoff diameter is about $6 \mu m$ (cf. Figure 7).

[39] For comparison, Table 1 summarizes the results of size dependent scattering measurements in the unperturbed marine boundary layer at different geographic locations. The measured Mace Head scattering coefficients are comparable to the reported total ($d \leq 10 \mu m$) scattering coefficients except for the higher scattering values observed during the Aerosol Characterization Experiment (ACE 1) in the SW Pacific Ocean. However, the SW Pacific Ocean measurements have taken place under a different wind regime with a higher mean wind speed of 9.7 m/s [De Bruyn *et al.*, 1998] compared to a mean value of 6.8 m/s during the Mace Head campaign and therefore favouring an enhanced sea salt aerosol production. In addition, the ACE 1 scattering coefficients are corrected for nephelometer nonidealities, resulting in on average 30% higher supermicrometer scattering coefficients [Quinn *et al.*, 1998], whereas no correction has been applied to the Mace Head data.

[40] Although the nephelometer measurements in Mace Head underestimate the light scattering, the detected scattering coefficients are in good agreement with results of similar measurements in the MBL. Hence the sampling characteristic of the nephelometer inlet at the observed wind speeds is comparable to the performance of the nominal 10 μm cutoff inlets.

Table 1. Measurements of Aerosol Scattering Coefficients in the Unperturbed MBL of Different Geographical Regions

Site	Range, Mm^{-1}	Mean, Mm^{-1}	Reference
Central Pacific Ocean ^a (RITS 94)	7.8–40	18.0 ± 6.8	Quinn <i>et al.</i> [1996]
Southwest Pacific Ocean (ACE 1)			Quinn <i>et al.</i> [1998]
$d \leq 1 \mu m$	0.66–38	4.4 ± 3	
$1 \mu m \leq d \leq 10 \mu m$	1.7–130	23 ± 16	
Southwest Pacific coast (Cape Grim)			Carrico <i>et al.</i> [1998]
$d \leq 1 \mu m$		3.6 ± 1.9	
$d \leq 10 \mu m$		15.4 ± 7.9	
Atlantic Ocean ^a (Aerosols99)			Quinn <i>et al.</i> [2001]
NH		16 ± 6.6	
SH tropics		13 ± 9.9	
East Atlantic coast Mace Head	2.8–82.9	20.8 ± 11.5	this work

^a Total scattering for $d \leq 10 \mu m$.

Table 2. Statistical Parameters of the Time Series of Measured Aerosol Scattering Coefficients (σ_{sp})

Time Period, Day of Year	Range, Mm^{-1}	Median, Mm^{-1}	Arithmetic mean, Mm^{-1}	Stdv (1σ), Mm^{-1}	n
156.0–164.1	2.8–16.1	8.0	8.2	2.8	166
164.2–171.5	8.4–49.6	21.2	21.7	7.7	177
171.5–174.9	5.0–17.6	11.4	11.0	3.4	82
175.0–177.4	16.8–82.9	28.3	33.1	13.8	59
177.7–184.0	2.9–31.9	11.1	12.6	6.5	153
Marine air masses ^a	2.8–82.9	18.7	20.8	11.5	352
Total	2.8–82.9	12.7	15.7	10.3	637

^a As defined by the local wind direction sector from 180° to 300° .

[41] The measured σ_{sp} time series in Figure 8 indicates 5 periods of different turbidity conditions with arithmetic mean values of up to a factor of 2 higher and lower than the overall mean of the σ_{sp} record. These periods are emphasized, by adding a 2-day running mean to the hourly averages. The statistical parameters of these periods, of marine air masses, as determined by the local wind direction, and of the total measurement period are summarized in Table 2.

3.3.1. Measured Scattering and Air Mass History

[42] The observed periods of varying mean scattering levels are associated with different air mass histories, as revealed by a trajectory analysis. The Irish Meteorological Service (MetÉireann) provides daily three-dimensional 5-day backward trajectories that arrive at Mace Head on the 975 hPa-level at 12 UTC. The trajectories are based on the Limited Area Trajectory Model of MetÉireann, which uses three-dimensional wind fields provided by the European Centre for Medium Range Weather Forecasts (ECMWF), [McGrath, 1989]. The periods 1 (DOY 156.0 – 164.1) and 2 (DOY 164.2 – 171.5) of the scattering coefficient time series are characterized by the advection of unperturbed air masses. However, the periods distinctively differ in their mean scattering levels with a factor of 2.6 higher mean light scattering coefficient during period 2 (cf. Table 2). The trajectory analysis shows that period 1 is dominated by arctic air masses with 75% of all trajectories originating north of Iceland. In addition, these trajectories show a slight subsidence from > 850 hPa. During period 2, 88% of all trajectories indicate air mass advection from the mid-Atlantic and thus characterizing a marine background air mass type. The back trajectories stayed fairly near to the ocean surface. Sample trajectories of these different air mass types and their vertical structures are presented in Figures 9a and b. For assessing the impact of the local wind speed, and hence the sea salt production on the scattering coefficients, Figure 10 presents the scattering coefficients of period 1 (triangles) and period 2 (squares) as a function of wind speed. Figure 10 demonstrates that for identical intervals of low wind speeds the period 2 scattering coefficients are enhanced compared to period 1 coefficients. Therefore the mean scattering level is predefined by the air mass history at moderate wind speeds with higher background scattering in marine air masses compared to arctic air masses.

[43] The periods 4 (DOY 175.0 – 177.4) and 5 (DOY 177.7 – 184.0) are dominated by perturbed marine air masses, that is 75% of all trajectories originate from the mid-Atlantic but passed landmasses before arriving at Mace

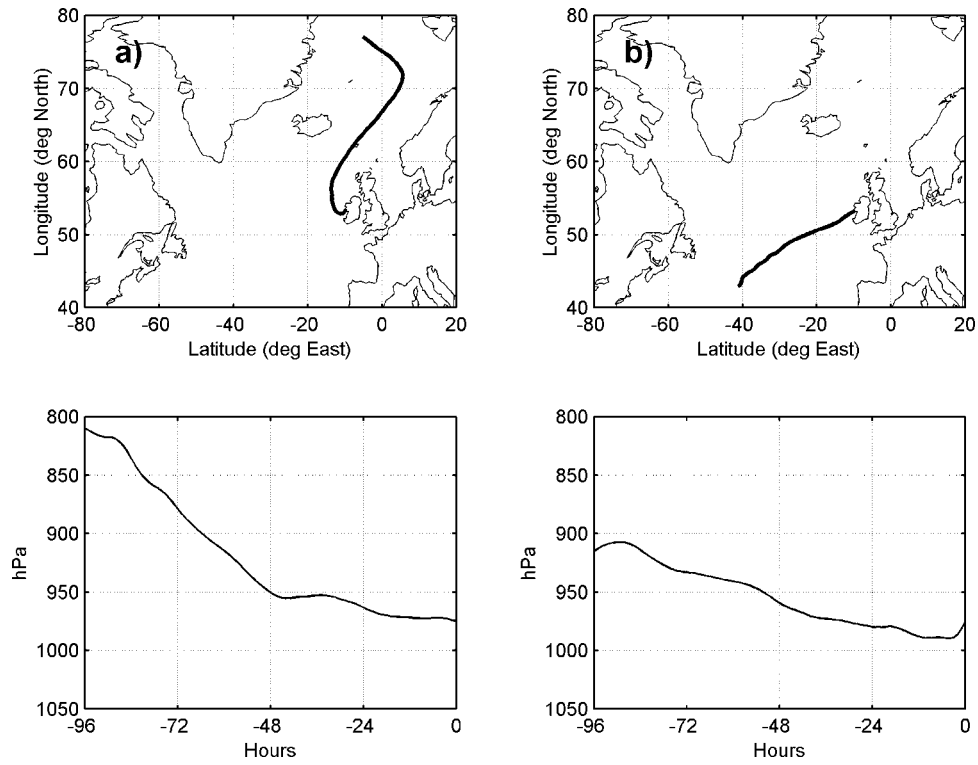


Figure 9. Backward trajectories (a) for arctic air masses at DOY 159 (8 June) and (b) for marine air masses at DOY 170 (19 June), arriving at Mace Head at 12 UTC.

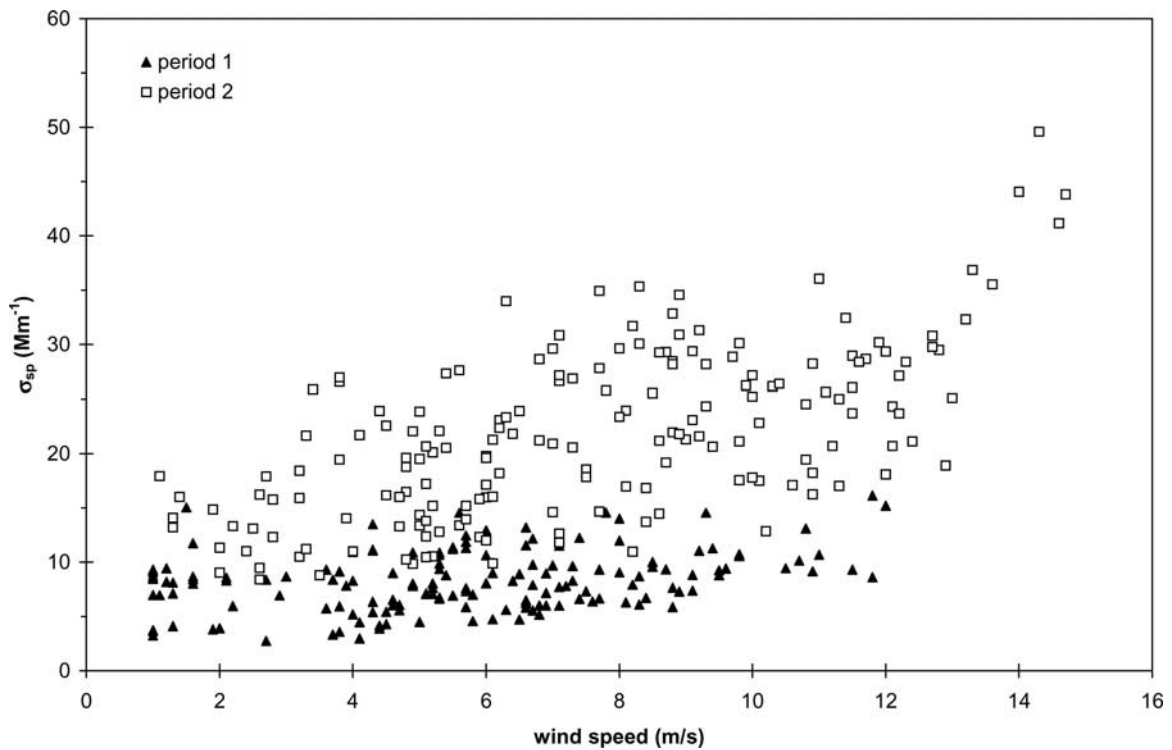


Figure 10. Measured scattering coefficients (σ_{sp}) of period 1 (triangles) and period 2 (squares) versus wind speed. Period 1 (DOY 156.0 – 164.1) is associated with the advection of arctic air masses whereas period 2 (DOY 164.2 – 171.5) is dominated by marine air masses.

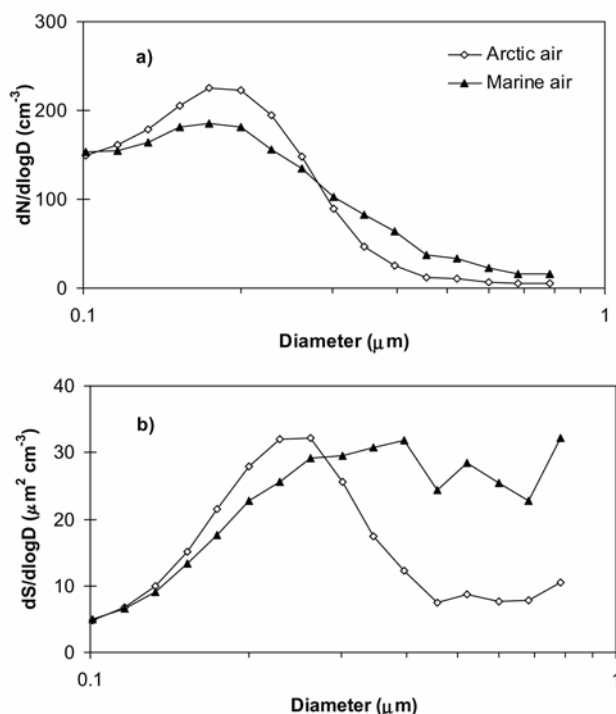


Figure 11. Mean (a) number and (b) surface size distributions for arctic and marine air masses for the periods DOY 156.0 – 164.1 and DOY 164.2 – 171.5, respectively.

Head. In addition, period 5 is influenced at least at 2 days (DOY 178 and 179) by arctic air masses. The prominent scattering peak at DOY 175 is caused by local bonfires which are traditionally lit during the St John's night from 23 to 24 June (DOY 174 – 175). Easterly wind directions

favoured the transport of the contaminants to the measurement site. Period 3 (DOY 171.5 – 174.9) has to be excluded from the analysis due to missing trajectory data.

[44] In general, a cluster analyses based on Mace Head scattering data for a period of 6 months reveals, that arctic air masses are associated with a factor of 1.8 lower scattering coefficients compared to marine air masses [O'Reilly *et al.*, 1999]. This corroborates the importance of the air mass history for the mean scattering levels.

[45] The periods 1 and 2, which are clearly defined by the advection of arctic and marine air masses, respectively, will be further investigated with regard to the particle distribution in the size range from 0.1 to 0.8 μm diameter, measured by the DMPS system. This size range is most important in radiative terms and is little affected by particle losses in the sampling system of the nephelometer (efficiency > 90%).

[46] A comparison of the normalized number and surface distribution for the arctic and the marine air mass type is presented in Figures 11a and 11b. The size distributions represent averages over the corresponding periods 1 and 2 and are normalized to a value of 100 cm^{-3} to facilitate the comparison. The aerosols of marine and arctic origin can be found to dominate the same mode, however in marine air masses $dN/d\log D$ is slightly larger for particles $>0.3\text{ }\mu\text{m}$ diameter. The distribution of particle surface area that defines the light scattering is indicated in Fig 11b. The aerosol surface area distribution in marine and arctic air masses diverges for particles $>0.3\text{ }\mu\text{m}$ diameter due to differences in particle number. However, the mean total surface area calculated for both periods is only slightly enhanced in the marine air mass, amounting to a value of $35\text{ }\mu\text{m}^2$ compared to $32\text{ }\mu\text{m}^2$ in the arctic air mass. Due to these similarities the observed difference in the background scattering signal has to be controlled by particles with diameters $d > 0.8\text{ }\mu\text{m}$.

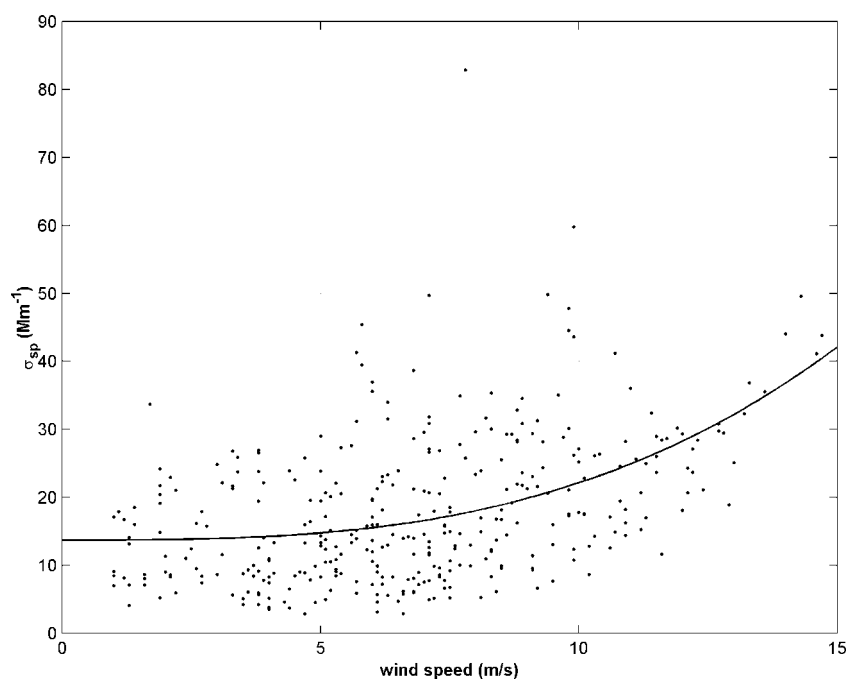


Figure 12. Measured scattering coefficient (σ_{sp}) versus local wind speed for marine air masses. Inserted is an exponential regression line ($r^2 = 0.20$).

3.3.2. Measured Scattering and Local Aerosol Sources

[47] In addition to the background scattering signal as defined by air mass history at low wind speeds, local sources will contribute to the total aerosol light scattering. Local aerosol sources that will be considered are the sea spray production, the aerosol plumes coming off the islands offshore of Mace Head as observed by lidar [Kunz *et al.*, 2002] and the secondary aerosol production due to biological emissions of the intertidal zone.

[48] The measured scattering within the marine sector is plotted against wind speed in Figure 12. An exponential regression line is added to the plot. The scattering coefficients exhibit a weak increase with increasing wind speed in excess of about 5 m/s, as indicated by the regression line. The wind speed-independent mean background scattering can be estimated from Figure 12 to amount to about 14 Mm^{-1} . The coefficient of determination is calculated to $r^2 = 0.20$. Therefore 20% of the variability in the data can be accounted for changes in wind speed, which is regarded as a proxy for the sea salt production process. The limitation of a wind speed correlation has been discussed above. In addition, the correlation is biased by the decreasing sampling efficiency of the inlet system with wind speed (cf. Figure 7). Since the measured scattering coefficients increase with wind speed, the enhanced sea spray production at higher wind speeds partly compensates for the inefficient sampling characteristics.

[49] Lidar studies [Kunz *et al.*, 2002] have shown that under certain wind conditions aerosol plumes generated by breaking waves at the islands off Mace Head can influence the measurement site. However, the plumes dominate the backscatter lidar signal only under low wind speed conditions, at higher wind speeds the signal of the sea spray aerosol produced by whitecaps overlaps the plume signal. The potential of the plumes to modify optical properties is exemplary illustrated for DOY 173 by Kunz *et al.* [2002]. On day of year 173 aerosol plumes are detected which originate from the island to the west of Mace Head (cf. Figure 1) and are transported to the measurement site by westerly winds. Analysis of the FSSP data for this day reveals that the particle concentrations are about a factor of 2 higher within the plume than under background conditions [Kunz *et al.*, 2002]. A comparison with the measured scattering coefficients shows that σ_{sp} increases from 7.8 Mm^{-1} (background conditions) to 16.3 Mm^{-1} (plume conditions), which is an increase of about a factor of 2. The calculated total scattering ($\sigma_{\text{sp, total}}$) is enhanced by a factor of 2.3 within the advected plume.

[50] The coastal zone near Mace Head is a strong source of newly formed particles and condensable vapours due to the enhanced biological emissions in the intertidal zone [O'Dowd *et al.*, 2002a]. These condensable vapours potentially can enhance the size of pre-existing particles, and consequently, their scattering properties. To examine if, during coastal nucleation events, the biogenic condensable vapours influence the scattering signal during the event, one of the most intensive nucleation events was investigated. During the nucleation event on DOY 163 (described in detail by O'Dowd *et al.* [2002b]), no enhancement in scattering was observed suggesting that tidal nucleation events do not influence the scattering measurements at Mace Head. It should be noted, however, that as the coastal

plume evolves over a period of 2–3 hours, a significant amount of new particles have grown to radiatively active sizes and increases in scattering and CCN ability, by more than a factor of two, can be achieved [O'Dowd, 2002].

4. Conclusions

[51] A time series of aerosol light scattering coefficients, covering the period of 1 month, has been investigated in conjunction with calculated scattering coefficients, based on measured aerosol size distributions and the application of Mie theory.

[52] The Mie calculation resulted in about one order of magnitude higher scattering coefficients for the MBL than have been measured until now. This was attributed to the additional mass of particles at $d > 10 \mu\text{m}$ which are typically excluded from the measurements but have been considered in the computation. Therefore a cutoff at $10 \mu\text{m}$ can lead to a significant underestimation of the light scattering. A comparison between the calculated total and submicrometer scattering coefficients revealed that on average 83% of the aerosol light scattering is attributed to supermicrometer particles.

[53] The reported measured scattering coefficients are underestimated by the nephelometer due to particle losses in the sampling system. The 50% cutoff diameter of the sampling system has been calculated to about $6 \mu\text{m}$ at the mean wind speed of the campaign of 6.8 m/s. However, a comparison of the Mace Head data with other MBL measurements showed a good agreement and thus indicating that the performance of the nephelometer inlet and nominal $10 \mu\text{m}$ cutoff inlets are similar.

[54] The measurements at Mace Head indicated that for moderate wind speeds the mean scattering level is defined by the air mass history. With increasing wind speed the sea spray production process got more pronounced and hence the background scattering signal was masked by the sea salt scattering signal. About 20% in the measured σ_{sp} variability could be explained by variations in wind speed and thus by variations in the sea salt production. This study has focused on the light scattering by dried aerosol particles as most previous measurements have done, to allow for comparisons. However, it has to be noted, that at ambient relative humidity the scattering coefficients will be significantly higher than reported here.

[55] **Acknowledgments.** The work is supported by the European Commission through the projects “New Particle Formation and Fate in the Coastal Environment (PARFORCE),” contract ENV4-CT-97-0526, “Synthesis of Integrated Global Aerosol Data Sets (SINGADS),” contract ENV4-CT-98-0780, and “Climate-Biosphere-Interactions (CORE),” contract EVRI-CT1999-40009. The work has also been conducted within the Environmental Change Institute (ECI) of the National University of Ireland, Galway under project CC-1.

References

- Anderson, T. L., and J. A. Ogren, Determining aerosol radiative properties using the TSI 3563 Integrating Nephelometer, *Aerosol Sci. Technol.*, **29**, 57–69, 1998.
- Anderson, T. L., et al., Performance characteristics of a high-sensitivity, three-wavelength, total scatter/backscatter nephelometer, *J. Atmos. Oceanic Technol.*, **13**, 967–986, 1996.
- Anderson, T. L., D. S. Covert, J. D. Wheeler, J. M. Harris, K. D. Perry, B. E. Trost, D. J. Jaffe, and J. A. Ogren, Aerosol backscatter fraction and single

- scatter albedo: Measured values and uncertainties at a coastal station in the Pacific Northwest, *J. Geophys. Res.*, *104*, 26,793–26,807, 1999.
- Bohren, C. F. and D. R. Huffman, *Absorption and Scattering of Light by Small Particles*, John Wiley, New York, 1983.
- Carrico, C. M., M. J. Rood, and J. A. Ogren, Aerosol light scattering properties at Cape Grim, Tasmania, during the First Aerosol Characterization Experiment (ACE 1), *J. Geophys. Res.*, *103*, 16,565–16,574, 1998.
- De Bruyn, W. J., T. S. Bates, J. M. Caine, and E. S. Saltzman, Shipboard measurements of dimethyl sulfide and SO₂ southwest of Tasmania during the First Aerosol Characterization Experiment (ACE 1), *J. Geophys. Res.*, *103*, 16,703–16,711, 1998.
- Exton, H. J., J. Latham, P. M. Park, S. J. Perry, M. H. Smith, and R. R. Allan, The production and dispersal of marine aerosol, *Q. J. R. Meteorol. Soc.*, *111*, 817–837, 1985.
- Fitzgerald, J. W., Marine aerosols: A review, *Atmos. Environ.*, *25A*, 533–545, 1991.
- Hänel, G., The properties of atmospheric aerosol particles as functions of the relative humidity at thermodynamic equilibrium with the surrounding moist air, *Adv. Geophys.*, *19*, 73–188, 1976.
- Hänel, G., and M. Lehmann, Equilibrium size of aerosol particles and relative humidity: New experimental data from various aerosol types and their treatment for cloud physics application, *Contrib. Atmos. Phys.*, *54*, 57–71, 1981.
- Horvath, H., Influence of atmospheric aerosols upon the global radiation balance, in *Atmospheric Particles*, edited by R. M. Harrison and R. E. van Grieken, pp. 543–596, John Wiley, New York, 1998.
- Intergovernmental Panel on Climate Change (IPCC), *Climate Change 1994*, edited by J. T. Houghton et al., Cambridge Univ. Press, New York, 1995.
- Jennings, S. G., M. Geever, F. M. McGovern, J. Francis, T. G. Spain, and T. Donaghy, Microphysical and physicochemical characterization of atmospheric marine and continental aerosol at Mace Head, *Atmos. Environ.*, *31*, 2795–2808, 1997.
- Kent, G. S., G. K. Yue, U. O. Farrukh, and A. Deepak, Modeling atmospheric aerosol backscatter at CO₂ laser wavelength, I, Aerosol properties, modeling techniques and associated problems, *Appl. Opt.*, *22*, 1655–1665, 1983.
- Krivácsy, Z., A. Hoffer, Z. Sárvári, D. Temesi, U. Baltensperger, S. Nyeki, E. Weingartner, S. Kleefeld, and S. G. Jennings, Role of organic and black carbon in the chemical composition of atmospheric aerosol at European background sites, *Atmos. Environ.*, *35*, 6231–6244, 2001.
- Kunz, G., G. de Leeuw, C. D. O'Dowd, and E. Becker, Lidar studies of the atmospheric boundary layer and locally generated sea spray aerosol plumes at Mace Head, *J. Geophys. Res.*, *107*, 10.1029/2001JD001240, in press, 2002.
- Latham, J., and M. Smith, Effect on global warming of wind-dependant aerosol generation at the ocean surface, *Nature*, *347*, 372–373, 1990.
- McGrath, R., Trajectory models and their use in the Irish Meteorological Service, *Internal Memo. 112/89*, Irish Meteorol. Serv. (Met Éireann), Glasnevin Hill, Dublin, 1989.
- Murphy, D. M., J. R. Anderson, P. K. Quinn, L. M. McInnes, F. J. Brechtel, S. M. Kreidenweis, A. M. Middlebrook, M. Posfai, D. S. Thomson, and P. R. Buseck, Influence of sea-salt on aerosol radiative properties in the Southern Ocean marine boundary layer, *Nature*, *392*, 62–65, 1998.
- O'Dowd, C. D., On the spatial extent and evolution of coastal aerosol plumes, *J. Geophys. Res.*, *107*, 10.1029/2001JD000422, in press, 2002.
- O'Dowd, C. D., and M. H. Smith, Physicochemical properties of aerosol over the northeast Atlantic: Evidence for wind speed related submicron sea-salt aerosol production, *J. Geophys. Res.*, *98*, 1137–1149, 1993.
- O'Dowd, C. D., M. H. Smith, and S. G. Jennings, Submicron particle, radon and soot carbon characteristics over the Northeast Atlantic, *J. Geophys. Res.*, *98*, 1123–1135, 1993.
- O'Dowd, C. D., M. H. Smith, I. E. Consterdine, and J. A. Lowe, Marine aerosol, sea-salt, and the marine sulphur cycle: A short review, *Atmos. Environ.*, *31*, 73–80, 1997.
- O'Dowd, C. D., M. Geever, M. K. Hill, S. G. Jennings, and M. H. Smith, New particle formation: Spatial scales and nucleation rates in the coastal environment, *Geophys. Res. Lett.*, *25*, 1661–1664, 1998.
- O'Dowd, C. D., J. A. Lowe, M. H. Smith, and A. D. Kaye, The relative importance of non-sea-salt sulphate and sea-salt-aerosol to the marine cloud condensation nuclei population: An improved multi-component aerosol-cloud droplet parameterization, *Q. J. R. Meteorol. Soc.*, *125*, 1295–1313, 1999a.
- O'Dowd, C. D., et al., On the photochemical production of new particles in the coastal boundary layer, *Geophys. Res. Lett.*, *26*, 1707–1710, 1999b.
- O'Dowd, C. D., et al., A dedicated study of New Particle Formation and Fate in the Coastal Environment (PARFORCE): Overview of objectives and achievements, *J. Geophys. Res.*, *107*, 10.1029/2001JD000555, in press, 2002a.
- O'Dowd, C. D., et al., Coastal new particle formation: Environmental conditions and aerosol physicochemical characteristics during nucleation bursts, *J. Geophys. Res.*, *107*, 10.1029/2000JD000206, in press, 2002b.
- O'Reilly, S., C. Kleefeld, and S. G. Jennings, Optical properties of the atmospheric aerosol at Mace Head, paper presented at the European Aerosol Conference, Prague, Czech Republic, 6–10 Sept., 1999.
- Pilinis, C., and X. Li, Particle shape and internal inhomogeneity effects on the optical properties of tropospheric aerosols of relevance to climate forcing, *J. Geophys. Res.*, *103*, 3789–3800, 1998.
- Quinn, P. K., V. N. Kapustin, T. S. Bates, and D. S. Covert, Chemical and optical properties of marine boundary layer aerosol particles of the mid-Pacific in relation to sources and meteorological transport, *J. Geophys. Res.*, *101*, 6931–6951, 1996.
- Quinn, P. K., D. J. Coffman, V. N. Kapustin, T. S. Bates, and D. S. Covert, Aerosol optical properties in the marine boundary layer during the First Aerosol Characterization Experiment (ACE 1) and the underlying chemical and physical aerosol properties, *J. Geophys. Res.*, *103*, 16,547–16,563, 1998.
- Quinn, P. K., D. J. Coffman, T. S. Bates, T. L. Miller, J. E. Johnson, K. Voss, E. J. Welton, and C. Neusüss, Dominant aerosol chemical components and their contribution to extinction during the Aerosols99 cruise across the Atlantic, *J. Geophys. Res.*, *106*, 20,783–20,810, 2001.
- Tang, I. N., Chemical and size effects of hygroscopic aerosols on light scattering coefficients, *J. Geophys. Res.*, *101*, 19,245–19,250, 1996.
- White, W. H., E. S. Macias, R. C. Nisinger, and D. Schorran, Size-resolved measurements of light scattering by ambient particles in the southwestern U.S.A., *Atmos. Environ.*, *28*, 909–921, 1994.
- Willeke, K., and P. A. Baron (Eds.), *Aerosol Measurement: Principles, Techniques, and Applications*, Van Nostrand Reinhold, New York, 1993.
- Van Dingenen, R., F. Raes, and N. R. Jensen, Evidence for anthropogenic impact on number concentration and sulfate content of cloud-processed aerosol particles over the North Atlantic, *J. Geophys. Res.*, *100*, 21,057–21,067, 1995.

P. Aalto and C. D. O'Dowd, Department of Physical Sciences, University of Helsinki, P.O. Box 9, Helsinki FIN-00014, Finland. (pasi.aalto@helsinki.fi; colin.odowd@emas.demon.co.uk)

E. Becker, 26 Andrew Lane, Hedon, Hull HU1 3DF, UK. (edo.becker@onetel.net.uk)

S. G. Jennings, C. Kleefeld, and S. O'Reilly, Department of Experimental Physics, National University of Ireland, University Road, Galway, Ireland. (Gerard.jennings@nuigalway.ie; sarah.oreilly@oxygen.ie; christoph.kleefeld@nuigalway.ie)

G. Kunz and G. de Leeuw, TNO Physics and Electronics Laboratory, P.O. Box 96864, N-2509 JG The Hague, Netherlands. (Deleeuw@fel.tno.nl; kunz@fel.tno.nl)